Theoretical Study of the Reaction Mechanism of HCN^+ and CH_4 of Relevance to Titan's Ion Chemistry

Yan Li, Hui-ling Liu, Xu-ri Huang,* Cai-yun Geng, Chia-chung Sun, and Au-chin Tang

State Key Laboratory of Theoretical and Computational Chemistry, Institute of Theoretical Chemistry, Jilin University, Changchun 130023, People's Republic of China

Received: October 15, 2007; In Final Form: December 6, 2007

Titan is the largest satellite of Saturn. In its atmosphere, CH_4 is the most abundant neutral after nitrogen. In this paper, the complex doublet potential-energy surface related to the reaction between HCN^+ and CH_4 is investigated at the B3LYP/6-311G(d,p), CCSD(T)/6-311G++(3df,2pd)(single-point), and QCISD/6-311G-(d,p) computational levels. A total of seven products are located on the PES. The initial association of HCN^+ with CH_4 is found to be a prereaction complex **1** ($HCNHCH_3^+$) without barrier. Starting from **1**, the most feasible pathway is the direct H-abstraction process (the internal C−H bond dissociation) leading to the product $\mathbf{P_1}$ ($HCNH^+ + CH_3$). By C−C addition, prereaction complex **1** can form intermediate **2** ($HNCHCH_3^+$) and then lead to the product $\mathbf{P_2}$ ($CH_3CNH^+ + H$). The rate-controlling step of this process is only 25.6 kcal/mol. It makes the Path $\mathbf{P_2}$ (1) $\mathbf{R \rightarrow 1 \rightarrow TS1/2 \rightarrow 2 \rightarrow TS2/P_2 \rightarrow P_2}$ another possible way for the reaction. $\mathbf{P_3}$ ($HCNCH_3^+ + H$), $\mathbf{P_5}$ ($cNCHCH_2^+ + H_2$), and $\mathbf{P_6}$ ($NCCH_3^+ + H_2$) are exothermic products, but they have higher barriers (more than 40.0 kcal/mol); $\mathbf{P_4}$ ($H + HCN + CH_3^+$) and $\mathbf{P_7}$ ($H + H_2 + HCCNH^+$) are endothermic products. They should be discovered under different experimental or interstellar conditions. The present study may be helpful for investigating the analogous ion−molecule reaction in Titan's atmosphere.

1. Introduction

Titan, the largest satellite of Saturn, is of considerable interest since its atmosphere is so various and it is one of the places where the most complex atmosphere organic chemistry takes place in the solar system. A number of investigations have been carried out to provide an understanding of the structure and composition of this atmosphere.[1−4] It has been established that the most abundant species in Titan's atmosphere is molecular nitrogen, followed by neutral methane. Solar radiation and energetic plasma from Saturn's magnetosphere ionizes the neutral molecules, creating an ionosphere at altitudes above 800 km.[5−12] The ion−molecule reactions that occur about the primary ions of N^+ and N_2^+ with CH_4 initiate the ion process and product ions of CH_2^+, CH_3^+, CH_4^+, and HCN^+. Then the ions react further with CH_4 and also with other hydrocarbons that are present in some abundance in Titan's atmosphere such as C_2H_2, C_2H_4, C_2H_6, etc. In this way, a complex matrix of reactions is quickly established with a wide range of products. Capone et al. suggested that simple organic−nitrogen compounds such as HCN are formed by cosmic ray bombardment in lower Titan's atmosphere (100−150 km),[13] and a mechanism of C_2H_2 with $HCNH^+$ has also been proposed by Capone et al.[14]

The ions and molecules chemistry in Titan's atmosphere are complex, which attracts chemists' and astronomers' attention. Several laboratory experimental techniques have been used to simulate the chemistry occurring in Titan's atmosphere. For example, McEwan, Anicich, and co-workers performed a lot of reactions using SIFT and ICR laboratory measurements.[15−18] Some theoretical investigations have also been done on the reactions of Titan's atmosphere, such as reactions of NH with CH_3[19] and N^+ ions with ethylene.[20] As one of the important ions in Titan's ionosphere, HCN^+ has drawn considerable attention, and many ion−molecule reactions relevant to HCN^+ have been investigated experimentally. In 2004, Anicich et al. performed an experiment on HCN^+ with CH_4, C_2H_2, and C_2H_4;[17] according to their experimental results, the products and distributions are

$$\begin{aligned} HCN^+ + CH_4 &\rightarrow HCNH^+ + CH_3 \quad 0.90 \\ &\rightarrow CH_4^+ + HCN \quad 0.04 \\ &\rightarrow CH_3CNH^+ + H \quad 0.03 \\ &\rightarrow CH_3^+ + HCN + H \quad 0.02 \\ &\rightarrow HCCNH^+ + H_2 + H \quad 0.01 \end{aligned}$$

However, to the best of our knowledge, there is no theoretical study on these reactions. In the present paper, we investigate a detailed theoretical study on the reaction mechanism of HCN^+ with CH_4.

2. Computational Methods

All calculations were performed using the Gaussian 98 program package.[21] The geometries of all the reactants, products, intermediates, and transition states are optimized using the popular density functional theory B3LYP[22] functions in conjunction with the d,p-polarized 6-311G(d,p) basis set. Frequency calculations were performed at the same level to check the obtained species is an isomer (with all real frequencies) or a transition state (with one and only one imaginary frequency).

10.1021/jp710006b CCC: $40.75
Published on Web 03/05/2008

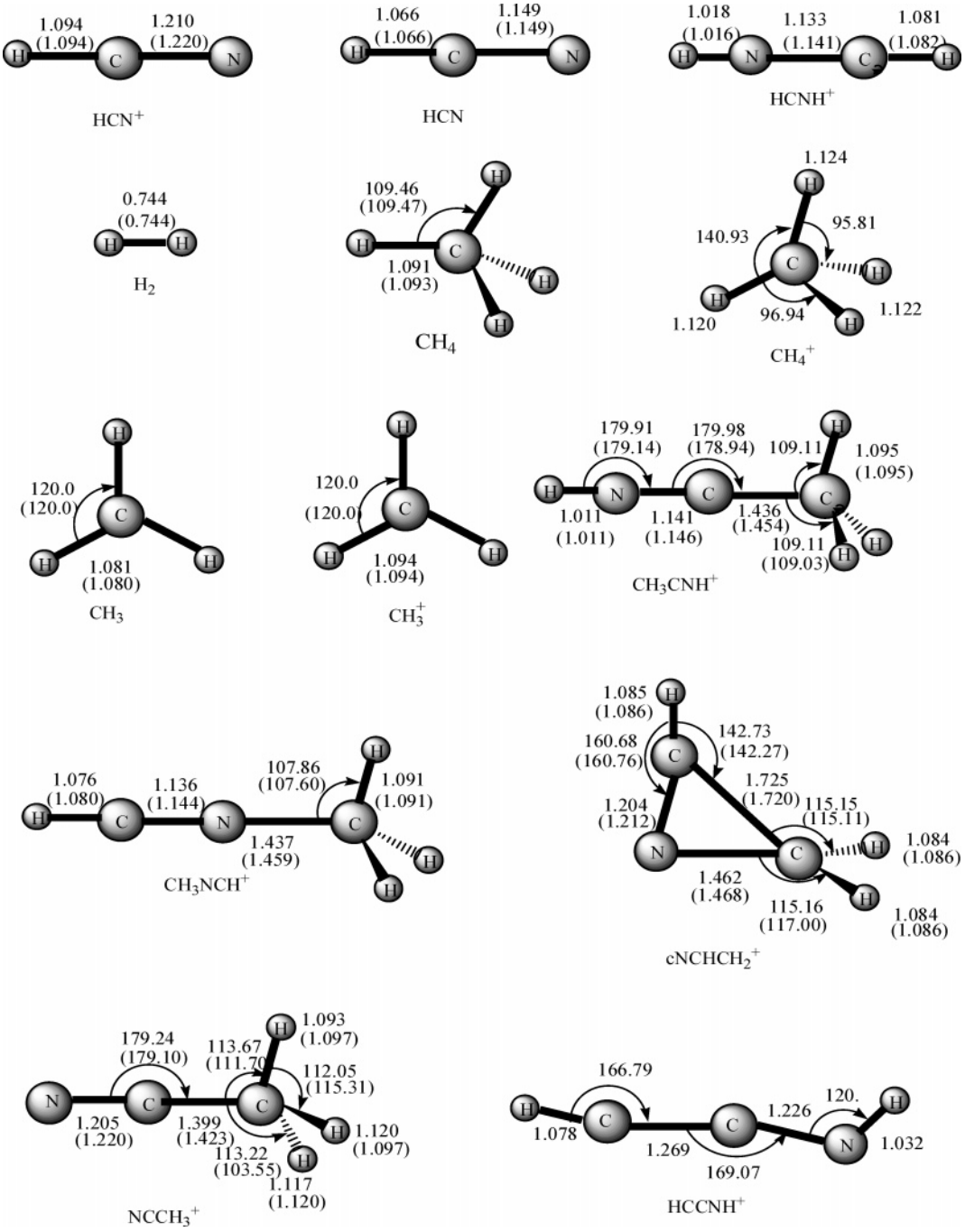

Figure 1. Optimized structures of the reactants and products at the B3LYP/6-311G(d,p) level. Distances are given in Angstroms and angles in degrees; the values in parentheses are at the QCISD/6-311G(d,p) level.

Intrinsic reaction coordinate (IRC)[23] calculations were performed at the B3LYP/6-311G(d,p) level to confirm that the transition state connects the designated intermediates. To obtain more reliable energetic data, single-point energy calculations were carried out at the CCSD(T)/6-311G++(3df,2pd)[24] level using the B3LYP/6-311G(d,p)-optimized geometries. For the favorite channels, the structures and energies were calculated at the CCSD(T)/6-311G++(3df,2pd)//QCISD/6-311G(d, p) level.

3. Results and Discussion

The optimized structures of reactants and products are shown in Figure 1, and the optimized structures of the intermediates and transition states are shown in Figures 2 and 3, respectively. The symbol **TSm/n** is used to denote the transition state connecting intermediates **m** and **n**. The energy of the reactant ($^2HCN^+ + {}^1CH_4$) is set to zero for reference. Unless stated otherwise, the relative energies mentioned hereafter refer to the CCSD(T)/6-311G++(3df,2pd)//B3LYP/6-311G(d,p)+ZPVE (zero-point vibrational energy) level. The relative energies including ZPVE corrections of all the species are listed in Table 1, and the CCSD(T)/6-311G++(3df,2pd)//QCISD/6-311G-(d,p)+ZPVE energetic values for some critical species are shown in Table 2. In addition, a schematic of the potential-energy surface (PES) of the $HCN^+ + CH_4$ reaction is depicted in Figure 4.

3.1. Reactant Channel Analysis. The reactant HCN^+ is a $^2\Sigma$ electronic state. Both of its single-electron and positive

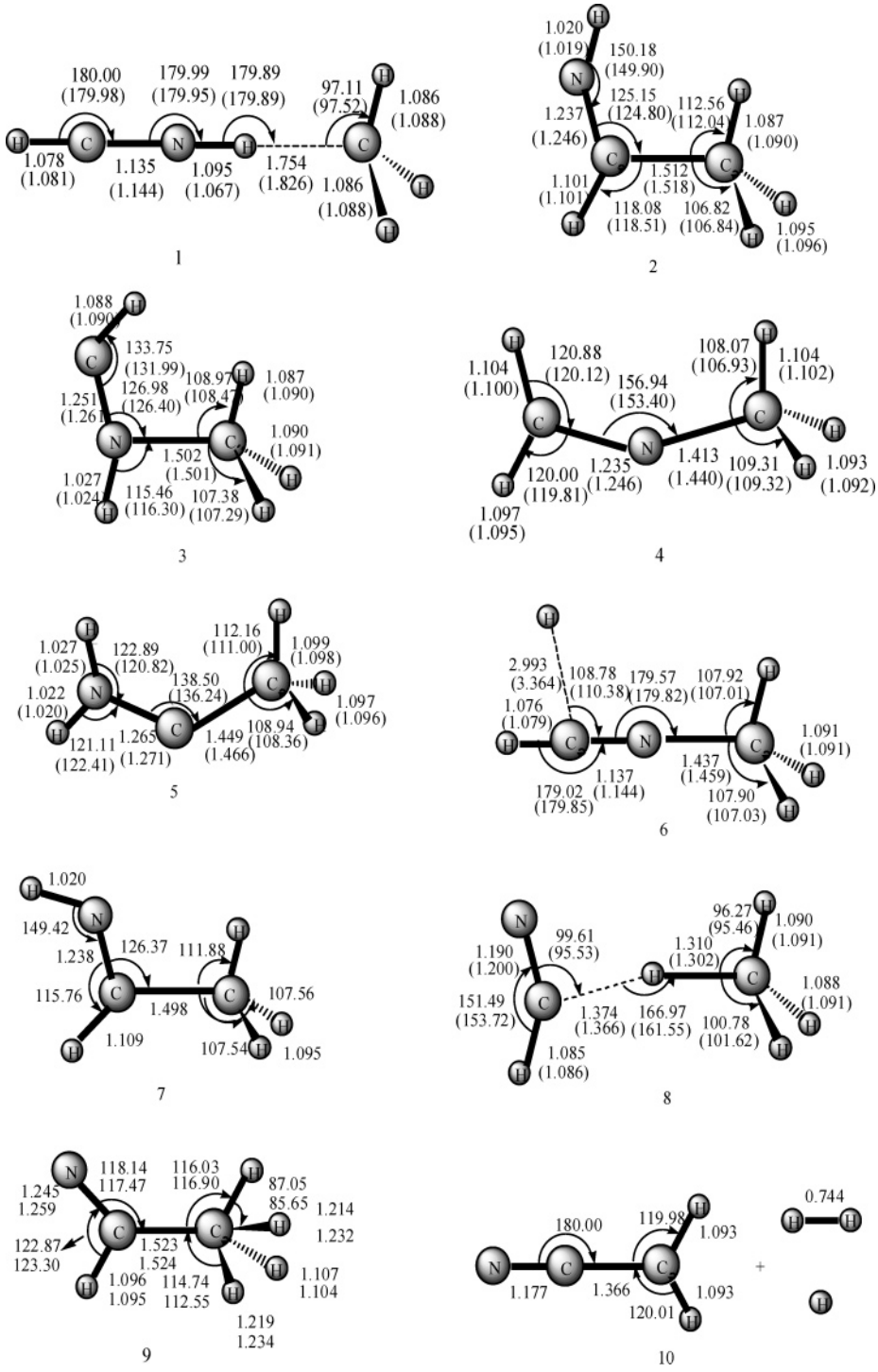

Figure 2. Optimized structures of the intermediates at the B3LYP/6-311G(d,p) level. Distances are given in Angstroms and angles in degrees. For the structures on the optimal channels, the values in parentheses are at the QCISD/6-311G(d,p) level.

electrical charge are focused on the terminal N atom, so the N atom is the active point of HCN^+. In Figure 4, the channels have been marked and the products listed. From Figure 4, we can see that the attack of the N atom on one H atom of the CH_4 molecule leads to a prereaction complex **1** ($HCNHCH_3^+$). The prereaction complex **1** is 75.5 kcal/mol more stable than the reactant, and all the pathways start from it; we also see that seven products are obtained. Among all the products, $\mathbf{P_4}$ and $\mathbf{P_7}$ are 16.4 and 46.4 kcal/mol higher than the reactant, respectively, while $\mathbf{P_1}$, $\mathbf{P_2}$, $\mathbf{P_3}$, $\mathbf{P_5}$, and $\mathbf{P_6}$ are 64.4, 76.3, 65.5, 29.4, and 27.4 kcal/mol lower than the reactant, respectively.

I. $\mathbf{P_1}$ (^{1}HCNH$^+$+^{2}CH$_3$). Path $\mathbf{P_1}$: R → 1 → $\mathbf{P_1}$. The product $\mathbf{P_1}$ ($^1HCNH^+ + {}^2CH_3$) is 64.4 (*65.4*) kcal/mol lower than the reactant, and it can be obtained via dissociation of prereaction complex **1** directly. The Italic value in parentheses is at the CCSD(T)//QCISD+ZPVE level. The internal C−H bond of prereaction complex **1** is 1.754 Å, 60% longer than other C−H bonds (about 1.08 Å) and easy to be broken. At the B3LYP/6-311G(d,p) level, no transition state is found during this process, and the corresponding scan for different C−H distance shows no sign of barrier at this level (as shown in Figure 5). Thus, we confirm that the process **1** → $\mathbf{P_1}$ is a direct H-extraction process without energy barrier.

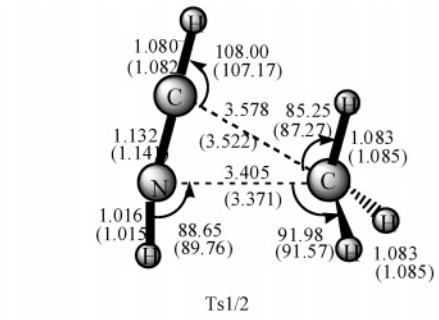

Ts1/2

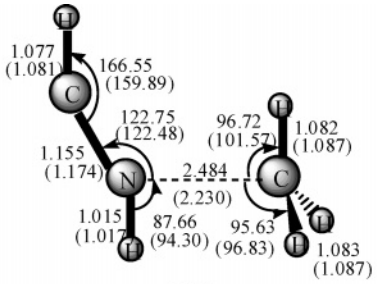

Ts1/3

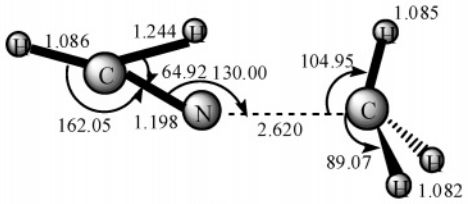

Ts1/4

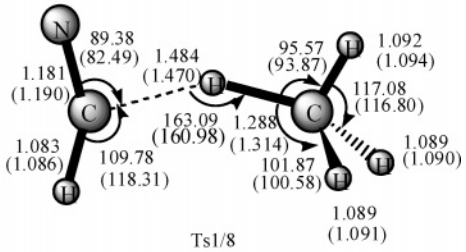

Ts1/8

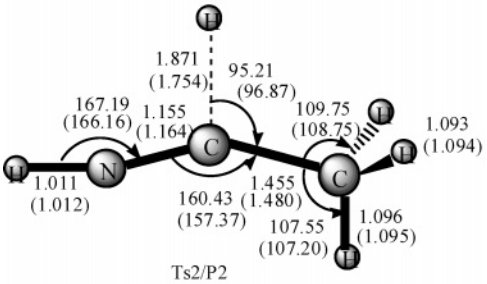

Ts2/P2

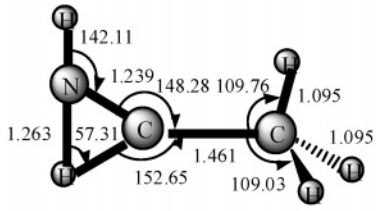

Ts2/5

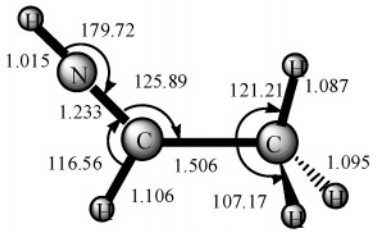

Ts2/7

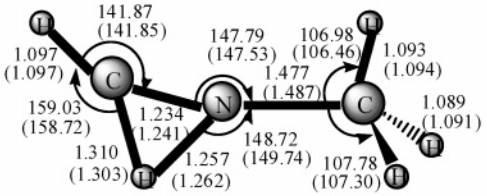

Ts3/4

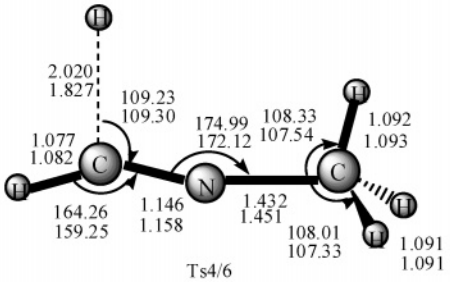

Ts4/6

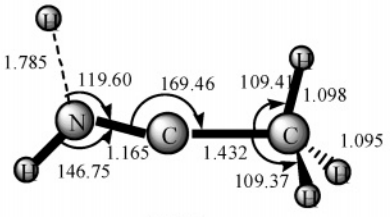

Ts5/P2

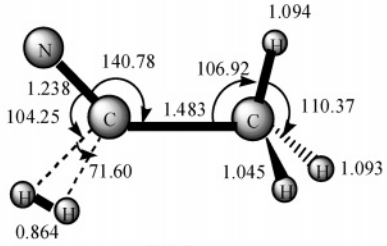

TS7/P6

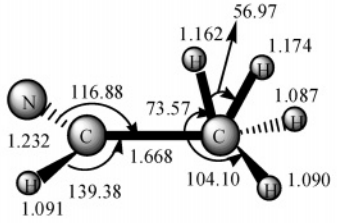

Ts8/9

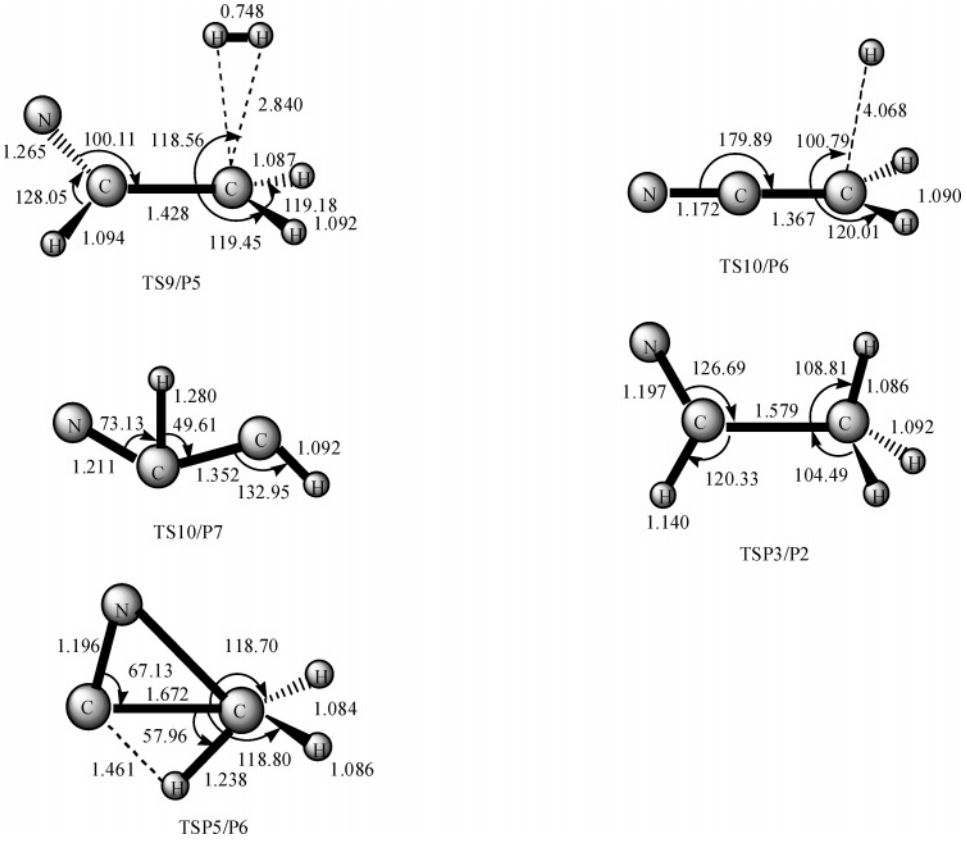

Figure 3. Optimized structures of the transition states at the B3LYP/6-311G(d,p) level. Distances are given in Angstroms and angles in degrees. For the structures on the optimal channels, the values in parentheses are at the QCISD/6-311G(d,p) level.

II. P_2($CH_3CNH^+ + H$). P_2 ($CH_3CNH^+ + H$) is the lowest lying product, which is 76.3 (*76.9*) kcal/mol lower than the reactant. We find three possible reaction pathways as follows

Path P_2 (1): $\mathbf{R \rightarrow 1 \rightarrow TS1/2 \rightarrow 2 \rightarrow TS2/P_2 \rightarrow P_2}$

Path P_2 (2): $\mathbf{R \rightarrow 1 \rightarrow TS1/2 \rightarrow 2 \rightarrow TS2/5 \rightarrow 5 \rightarrow TS5/P_2 \rightarrow P_2}$

Path P_2 (3): $\mathbf{P_3 \rightarrow TSP_3/P_2 \rightarrow P_2}$

The product $\mathbf{P_2}$ can be obtained from dissociation of the C−H and N−H bond of intermediates **2** and **5**, respectively. Intermediate **2** can be produced by complex **1** via an internal C−H bond being broken and a C−C bond being formed. Since the high-energy barrier step controls the reaction rate in a pathway, the step $\mathbf{2 \rightarrow TS2/P_2}$ can be viewed as the rate-controlling step of this path given that the barrier (25.6, *26.0* kcal/mol) of it is higher than the other step (8.3, *10.5* kcal/mol for **1** → TS**1**/**2**). Intermediate **5** can be obtained from intermediate **2** via a 2,3 H shift (from the C atom to the N atom) and then an H-elimination process leading to $\mathbf{P_2}$. Obviously, $\mathbf{2 \rightarrow TS2/5}$ can be seen as the rate-controlling step for **Path P_2 (2)**, and the activation energy of $\mathbf{2 \rightarrow TS2/5}$ is 41.1 kcal/mol. The third way to form $\mathbf{P_2}$ is a secondary reaction, and it can be obtained from $\mathbf{P_3}$ ($HCNCH_3^+ + H$) via an isomerization process. The transition state $\mathbf{TSP_3/P_2}$ is 1.6 kcal/mol higher than the reactant, and the barrier of $\mathbf{P_3 \rightarrow TSP_3/P_2}$ is 67.1 kcal/mol. Among the three channels, the optimal one is **Path P_2 (1)** with an activation energy of 25.6 (*26.0*) kcal/mol.

III. P_3 ($HCNCH_3^+$+H). Product $\mathbf{P_3}$ is 65.5 (*66.1*) kcal/mol more stable than the reactant. There are three possible pathways to generate it.

Path P_3 (1): $\mathbf{R \rightarrow 1 \rightarrow TS1/4 \rightarrow 4 \rightarrow TS4/6 \rightarrow 6 \rightarrow P_3}$

Path P_3 (2): $\mathbf{R \rightarrow 1 \rightarrow TS1/3 \rightarrow 3 \rightarrow TS3/4 \rightarrow 4 \rightarrow TS4/6 \rightarrow 6 \rightarrow P_3}$

Path P_3 (3): $\mathbf{P_2 \rightarrow TSP_3/P_2 \rightarrow P_3}$

The product $\mathbf{P_3}$ can be obtained from intermediate **4** via a C−H bond elongatation to form intermediate **6** (the C−H bond lengthens to 2.993 Å) and then an H-elimination process. Intermediate **4** can be viewed as the internal C−H bond of complex **1** cleaves and the C−N bond is formed; at the same time, the internal H atom transfers from the N to the C atom. This is the rate-controlling step of **Path P_3 (1)**, and the barrier of $\mathbf{1 \rightarrow TS1/4}$ is 53.8 kcal/mol. There is another way (**Path P_3 (2)**) to form intermediate **4**. From prereaction complex **1**, the internal C−H bond is broken and the C−N bond formed to generate intermediate **3**. After that, the internal H atom shifts from the N atom to the C atom. In **Path P_3 (2)**, the rate-controlling step is $\mathbf{3 \rightarrow TS3/4}$, which is 44.8 kcal/mol and more likely to be followed than **Path P_3 (1)**. The third way to obtain $\mathbf{P_3}$ is $\mathbf{P_2}$ isomerization to $\mathbf{P_3}$. The barrier of $\mathbf{P_2 \rightarrow TSP_3/P_2}$ is high to 77.9 kcal/mol. Thus, the optimal channel to generate $\mathbf{P_3}$ is **Path P_3 (2)**.

IV. P_4 (H+HCN+CH_3^+). Product $\mathbf{P_4}$ is 16.4 kcal/mol higher than the reactant. The only way to generate it is

Path P_4: $\mathbf{P_3 \rightarrow P_4}$

TABLE 1: Energies of the Reactants, Products, Intermediatesm and Transition States at the B3LYP/6-311G(d,p) and CCSD(T)/6-311G++(3df,2pd)//B3LYP/6-311G(d,p) Levels (in au; the values in parentheses and total column are relative energies in kcal/mol)

species	B3LYP	ZPVE	CCSD//B3LYP	total
R ($^2HCN^+ + {}^1CH_4$)	−133.48904	37.20152 (0.0)	−133.21720 (0.0)	0.0
P$_1$($HCNH^+ + CH_3$)	−133.58692	36.05638 (−1.1)	−133.31804 (−63.3)	−64.4
P$_2$($CH_3CNH^+ + H$)	−133.60562	35.03538 (−2.2)	−133.33533 (−74.1)	−76.3
P$_3$ ($HCNCH_3^+ + H$)	−133.58713	35.48736 (−1.7)	−133.31878 (−63.7)	−65.5
P$_4$ ($CH_3^+ + HCN + H$)	−133.44554	29.89384 (−7.3)	−133.17937 (23.7)	16.4
P$_5$ ($cNCHCH_2^+ + H_2$)	−133.52996	32.98985 (−4.2)	−133.25741 (−25.2)	−29.4
P$_6$($NCCH_3^+ + H_2$)	−133.53279	31.18823 (−6.0)	−133.25136 (−21.4)	−27.4
P$_7$($HCCNH^+ + H_2 + H$)	−133.39966	24.73842 (−12.5)	−133.12336 (58.9)	46.4
CT($HCN + CH_4^+$)	−133.51926	32.95958 (−4.2)	−133.24107 (−15.0)	−19.2
1	−133.60842	36.93844 (−0.3)	−133.33702 (−75.2)	−75.5
2	−133.64958	40.80090 (−3.6)	−133.37281 (−97.6)	−94.0
3	−133.64045	42.67504 (−5.5)	−133.36732 (−94.2)	−88.7
4	−133.65211	40.67285 (−3.5)	−133.37348 (−98.1)	−94.6
5	−133.66751	42.22524 (−5.0)	−133.39005 (−108.5)	−103.4
6	−133.58766	35.81411 (−1.4)	−133.31947 (−64.2)	−65.6
7	−133.64978	40.64680 (−3.4)	−133.37288 (−97.7)	−94.2
8	−133.55260	35.53261 (−1.7)	−133.27194 (−34.3)	−36.0
9	−133.53820	37.61322 (−0.4)	−133.26491 (−29.9)	−29.5
10	−133.43658	26.11421 (−11.1)	−133.16279 (34.1)	23.1
TS1/2	−133.59192	36.94376 (−0.3)	−133.32391 (−67.0)	−67.2
TS1/3	−133.59177	37.21345 (0.0)	−133.31516 (−61.5)	−61.5
TS1/4	−133.50951	33.96213 (−3.2)	−133.23073 (−8.5)	−11.7
TS1/8	−133.55246	34.99873 (−2.2)	−133.27220 (−34.5)	−36.7
TS2/P$_2$	−133.59832	35.96654 (−1.2)	−133.32425 (−67.2)	−68.4
TS2/5	−133.57874	37.35117 (−0.1)	−133.30174 (−53.0)	−52.9
TS2/7	−133.64785	39.75929 (−2.6)	−133.37069 (−96.3)	−93.8
TS3/4	−133.56318	37.86122 (−0.7)	−133.28817 (−44.5)	−43.9
TS4/6	−133.58508	35.97926 (−1.2)	−133.31247 (−59.8)	−61.0
TS5/P$_2$	−133.59481	35.78693 (−1.4)	−133.31692 (−62.6)	−64.0
TS7/P$_6$	−133.53084	36.09752 (−1.1)	−133.25465 (−23.5)	−24.6
TS8/9	−133.53595	36.90786 (−0.3)	−133.26029 (−27.0)	−27.3
TS9/P$_5$	−133.51592	33.38434 (−3.8)	−133.23872 (−13.5)	−17.3
TS10/P$_7$	−133.27987	21.09764 (−16.1)	−133.00992 (130.1)	114.0
TSP$_3$/P$_2$	−133.48453	32.46125 (−4.7)	−133.21219 (−3.1)	−1.6
TSP$_5$/P$_6$	−133.44830	30.86210 (−6.3)	−133.17984 (23.4)	17.1
TS10/P$_6$	−133.44318	26.38106 (−10.8)	−133.16335 (33.8)	23.0

TABLE 2: Energies of the Structures on the Optimal Channels at the CCSD(T)/6-311G++(3df,2pd)//B3LYP/6-311G(d,p)+ZPVE and CCSD(T)/6-311G++ (3df,2pd)//QCISD/6-311G(d,p)+ZPVE Levels (in au; the values in parentheses and total columns are relative energies in kcal/mol)

species	CCSD(T)//B3LYP	total 1	CCSD(T)//QCISD	total 2
R	−133.21720 (0.0)	0.0	−133.21722 (0.0)	0.0
1	−133.33702 (−75.2)	−75.5	−133.33730 (−75.3)	−75.9
2	−133.37281 (−97.6)	−94.0	−133.37283 (−97.6)	−94.3
3	−133.36732 (−94.2)	−88.7	−133.36739 (−94.2)	−89.1
4	−133.37348 (−98.1)	−94.6	−133.37364 (−98.2)	−94.8
6	−133.31947 (−64.2)	−65.6	−133.31947 (−64.2)	−66.4
7	−133.37288 (−97.7)	−94.2	−133.37289 (−97.7)	−94.5
8	−133.27194 (−34.3)	−36.0	−133.27237 (−34.6)	−36.4
9	−133.26491 (−29.9)	−29.5	−133.26503 (−30.0)	−29.7
P$_1$	−133.31804 (−63.3)	−64.4	−133.31819 (−63.4)	−65.4
P$_2$	−133.33533 (−74.1)	−76.3	−133.33552 (−74.2)	−76.9
P$_3$	−133.31878 (−63.7)	−65.5	−133.31888 (−63.8)	−66.1
P$_5$	−133.25741 (−25.2)	−29.4	−133.25765 (−25.4)	−30.4
P$_6$	−133.25136 (−21.4)	−27.4	−133.25203 (−21.8)	−27.9
TS1/2	−133.32391 (−67.0)	−67.2	−133.32400 (−67.0)	−68.1
TS1/3	−133.31516 (−61.5)	−61.5	−133.31198 (−59.5)	−59.6
TS1/8	−133.27220 (−34.5)	−36.7	−133.27279 (−34.9)	−37.2
TS2/P$_2$	−133.32425 (−67.2)	−68.4	−133.32335 (−66.6)	−68.3
TS2/7	−133.37069 (−96.3)	−93.8	−133.37069 (−96.3)	−94.1
TS3/4	−133.28817 (−44.5)	−43.9	−133.28818 (−44.5)	−44.3
TS4/6	−133.31247 (−59.8)	−61.0	−133.31098 (−58.8)	−60.5
TS7/P$_6$	−133.25465 (−23.5)	−24.6	−133.25591 (−24.3)	−25.2
TS8/9	−133.26029 (−27.0)	−27.3	−133.26058 (−27.2)	−27.5

The channel to form product **P$_3$** has been discussed in III, and the NC bond of P_3 being broken directly leads to **P$_4$**.

V. P$_5$ ($cNCHCH_2^+ + H_2$). The product **P$_5$** is 29.4 kcal/mol more stable than the reactant. The way to form product **P$_5$** is as follows

Path P$_5$: R → 1 → TS1/8 → 8 → TS8/9 → 9 → TS9/P$_5$ → P$_5$

As it can be seen from the schematic of PES, **P$_5$** can be obtained from intermediate **9** via the C−N bond formed incorporating with two H atoms eliminated as an H_2 molecule. On the PES, we can see that intermediate **8** can transform to intermediate **9** via breaking one of the internal C−H bonds and forming the CC bond. Since the transition state **TS1/8** lies lower than **8**, intermediate **8** may be not a stationary point and the prereaction complex **1** can generate intermediate **9** directly. The rate-controlling step may be **1 → TS8/9**, and the barrier is 48.2 kcal/mol.

VI. P$_6$ ($NCCH_3^+ + H_2$). The product **P$_6$** lies 27.4 kcal/mol lower than the reactant. It can be generated via the following steps

Path P$_6$ (1): R → 1 → TS1/2 → 2 → TS2/7 → 7 → TS7/P$_6$ → P$_6$

Path P$_6$ (2): P$_5$ → TS P$_5$/P$_6$ → P$_6$

In the first channel, intermediate **2** can be produced by complex **1** via an internal C−H bond being broken and a C−C bond

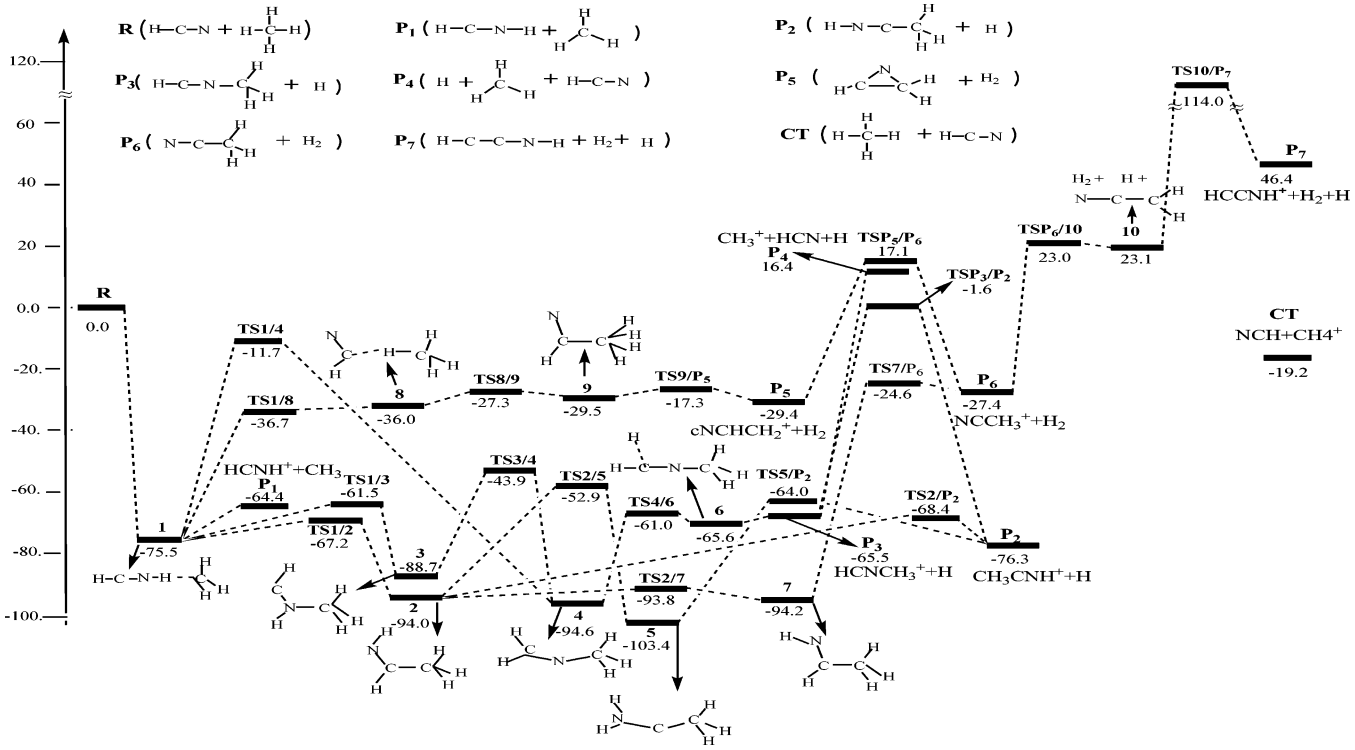

Figure 4. Sketch map of the potential-energy surface (PES).

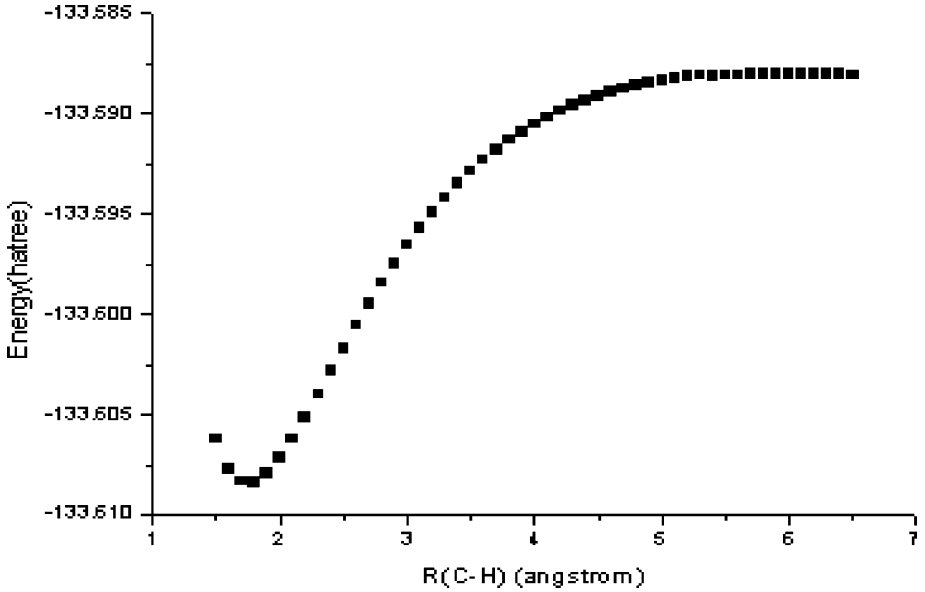

Figure 5. Dissociation curve of 1_P1 computed at the B3LYP/6-311G(d,p) level. The horizontal line denotes the energy *P*1.

being formed. The transformation of **2** → **7** is a N−H rotation process (around N−C bond), and then the H atom bonded to N transfers to the internal C atom and is eliminated as a H_2 molecule with the H on the C to generate $\mathbf{P_6}$. We can see from the schematic of the PES that the pathway must overcome a high barrier of 69.6 kcal/mol (**7** → **TS7/P6**) to form $\mathbf{P_6}$. The second way is a cyclic opening and an H-shift process from $\mathbf{P_5}$. Although the energy barrier in **Path P6 (2)** is lower than **Path P6 (1)**, the transition state **TSP5/P6** is 17.1 kcal/mol higher than the reactant, so we viewed **Path P6 (1)** as the main channel to form $\mathbf{P_6}$ with an activation energy of 69.6 kcal/mol.

VII. P_7 ($H + H_2 + HCCNH^+$). Product $\mathbf{P_7}$ is 46.4 kcal/mol higher than the reactant. It can be formed via product $\mathbf{P_6}$ in the following way

Path P_7: P_6 → $TSP_6/10$ → 10 → $TS10/P_7$ → P_7

$\mathbf{P_6}$ is $NCCH_3^+ + H_2$, and the way to generate it has been discussed in VI. Its H-elimination process forms intermediate **10** and then via rearrangement yields $\mathbf{P_7}$. The energy barriers of the two processes are 50.5 and 90.9 kcal/mol, respectively. Thus, the rate-controlling step is **10** → **TS10/P7** with an activation energy of 90.9 kcal/mol.

3.2. Charge-Transfer Channel. According to the experimental investigation of Anicich et al., a charge-transfer product (CT) $CH_4^+ + HCN$ has been detected. In our calculation, this channel has not been found. However, we can see in Table 1 that this CT product is 19.2 kcal/mol lower than the reactant and that this exothermic reaction may be generated via long-range collisions, and therefore, it should be a competitive channel.

3.3. Product Analysis. Comparing every optimal channel of forming possible products, we found that the energy barrier order of the rate-controlling step increases as follows: **Path P_1** → **Path P_2 (1)** (25.6) → **Path P_3 (2)** (44.8) → **Path P_4** (44.8) → **Path P_5** (48.2) → **Path P_6** (1) (69.6) → **Path P_7** (90.9). Since the energy of the barrier determines the reaction rate of the product, the rate order should be **P_1** ($HCNH^+ + CH_3$) > **P_2** ($CH_3CNH^+ + H$) > **P_3** ($HCNCH_3^+ + H$) > **P_4** ($CH_3^+ + HCN + H$) > **P_5** ($cNCHCH_2^+ + H_2$) > **P_6** ($NCCH_3^+ + H_2$) > **P_7** ($HCCNH^+ + H_2 + H$). Considering that **P_4** ($CH_3^+ + HCN + H$) is the second-order product of **P_3** and **P_7** ($HCCNH^+ + H_2 + H$) is the second-order product of **P_5** and **P_6**, **P_3** may dissociate to **P_4** ($CH_3^+ + HCN + H$) whereas **P_5** and **P_6** may dissociate to **P_7** ($HCCNH^+ + H_2 + H$) at high-temperature experimental conditions, so the final products may be **P_1** ($HCNH^+ + CH_3$) > **P_2** ($CH_3CNH^+ + H$) > **P_4** ($CH_3^+ + HCN + H$) > **P_7** ($HCCNH^+ + H_2 + H$), while at low-temperature experimental conditions the exothermic products **P_3**, **P_5**, and **P_6** should be found in the experimental process instead of **P_4** and **P_7**, and the final products may be **P_1** ($HCNH^+ + CH_3$) > **P_2** ($CH_3CNH^+ + H$) > **P_3** ($HCNCH_3^+ + H$) > **P_5** ($cNCHCH_2^+ + H_2$) > **P_6** ($NCCH_3^+ + H_2$). In addition, it should be mentioned that the charge-transfer product **CT** ($HCN + CH_4^+$) should be a competitive product too.

In 2004, Anicich et al. performed experimental studies on the reaction $HCN^+ + CH_4$ using the flowing afterglow-selected ion flow tube (FA-SIFT) at room temperature. The experimental results show the products and distributions as $HCNH^+ + CH_3$ (0.90) > $CH_4^+ + HCN$ (0.04) > $CH_3CNH^+ + H$ (0.03) > $CH_3^+ + HCN + H$ (0.02) > $HCCNH^+ + H_2 + H$ (0.01). Among the products, $HCNH^+ + CH_3$ corresponds to **P_1** in our result and the distribution is much higher than other products. $CH_3CNH^+ + H$ corresponds to **P_2** in our study. $CH_3^+ + HCN + H$ and $HCCNH^+ + H_2 + H$ correspond to **P_4** and **P_7**, respectively. This result is in good agreement with our calculations. However, the low temperature in Titan's atmosphere is about 170 K, and its surface temperature is 96 K,[25] so in our opinion, the products **P_3** ($HCNCH_3^+ + H$), **P_5** ($cNCHCH_2^+ + H_2$), and **P_6** ($NCCH_3^+ + H_2$) should also exist in interstellar space.

The energies of the reactant, intermediates, transition states, and products may be different at the different temperatures. Most of the pathways on the PES (as shown in Figure 4) are exothermic channels, and the increase of the temperature from 0 to 170 K may make these channels easier to proceed. However, considering that the temperature in Titan's atmosphere is low, the energy correction for temperature may be not play a great role.

4. Assessment of Computational Reliability

We performed additional calculations for the critical species of some reaction channels at the QCISD/6-311G(d,p) level, and we expected the more expensive method QCISD to be superior to the B3LYP method. As shown in Figures 1−3, the structural parameters at the two levels are general in agreement with each other and most importantly as shown in Table 2 the relative energies of the 23 species calculated at CCSD(T)//B3LYP+ZPVE and CCSD(T)//QCISD+ZPVE are close to each other with the largest deviation 1.9 kcal/mol of **TS1/3**. Thus, the present computational method is expected to provide reliable mechanistic information for $HCN^+ + CH_4$ reaction.

5. Conclusion

A detailed theoretical investigation has been carried out on the reaction of $HCN^+ + CH_4$; the result can be summarized as follows: starting from the reactant, a prereaction complex **1** is formed, **1** can undergo H transfer leading to **P_1** ($HCNH^+ + CH_3$), which is a direct process. Besides **P_1**, there are other six products **P_2** ($CH_3CNH^+ + H$), **P_3** ($HCNCH_3^+ + H$), **P_4** ($HCN + CH_3^+ + H$), **P_5** ($cNCHCH_2^+ + H_2$), **P_6** ($NCCH_3^+ + H_2$), and **P_7** ($HCCNH^+ + H_2 + H$). The energies of the rate-controlling steps are increased in turn. At high-temperature experimental conditions, the final products may be **P_1** ($HCNH^+ + CH_3$) > **P_2** ($CH_3CNH^+ + H$) > **P_4** ($HCN + CH_3^+ + H$) > **P_7** ($HCCNH^+ + H_2 + H$); at low-temperature experimental conditions, the final products may be **P_1** ($HCNH^+ + CH_3$) > **P_2** ($CH_3CNH^+ + H$) > **P_3** ($HCNCH_3^+ + H$) > **P_5** ($cNCHCH_2^+ + H_2$) > **P_6** ($NCCH_3^+ + H_2$). The conclusions are in good agreement with the experimental investigation, and we hope the results may provide useful information for understanding the ion−molecule reaction in Titan's atmosphere.

Acknowledgment. This work was supported by the National Natural Science Foundation of China (No20773048).

References and Notes

(1) Bauer, S. J. *Adv. Space Res.* **1987**, *7*, 65.

(2) Cravens, T. E.; Robertson, I. P.; Waite, J. H.; Yelle, R. V.; Kasprzak, W. T.; Keller, C. N.; Ledvina, S. A.; Niemann, H. B.; Luhmann, J. G.; McNutt, R. L.; Ip, W. H.; DeLaHaye, V.; Mueller-Wodarg, I.; Wahlund, J. E.; Anicich, V. G.; Vuitton, V. *Geophys. Res. Lett.* **2006**, *33* (7), Art. No. L07105.

(3) Fulchignoni, M.; Ferri, F.; Angrilli, F.; Ball. A. J.; Bar-Nun, A.; Barucci, M. A.; Bettanini, C.; Bianchini, G.; Borucki, W.; Colombatti, G.; Coradini, M.; Coustenis, A.; Debei, S.; Falkner, P.; Fanti, G.; Flamini, E.; Gaborit, V.; Grard, R.; Hamelin, M.; Harri, M. A.; Hathi, B.; Jernej, I.; Leese, M. R.; Lehto, A.; Lion Stoppato, P. F. López-Moreno, J. J.; Mäkinen, T.; McDonnell, J. A. M.; McKay, C. P.; Molina-Cuberos, G.; Neubauer, F. M. Pirronello, V.; Rodrigo, R.; Saggin, B.; Schwingenschuh, K.; Seiff, A.; Simões, F. Svedhem, H.; Tokano, T.; Towner, M. C.; Trautner, R.; Withers, P.; Zarnecki. J. C. *Nature* **2006**, *438*, 785.

(4) Vuitton, V.; Yelle, R. V.; McEwan, M. J. *Icarus* **2007**, *191*, 722.

(5) Bird, M. K.; Dutta-Roy, R.; Asmar, S. W.; Rebold, T. A. *Icarus* **1997**, *130*, 426.

(6) Wahlund, J.-E.; Boström, R.; Gustafsson, G.; Gurnett, D. A.; Kurth, W. S.; Pedersen, A.; Averkamp, T. F.; Hospodarsky, G. B.; Personn, A. M.; Canu, P.; Neubauer, F. M.; Dougherty, M. K.; Eriksson, A. I.; Morooka, M. W.; Gill, R.; André, M.; Eliasson, L.; Müller-Wodarg, I. *Science* **2005**, *308*, 986.

(7) Keller, C. N.; Cravens, T. E.; Gan, L. *J. Geophys. Res.* **1992**, *97*, 12117.

(8) Gan, L.; Keller, C. N.; Cravens, T. E. *J. Geophys. Re* **1992**, *97*, 12136.

(9) Cravens, T. E.; Robertson, I. P.; Clark, J.; Wahlund, J.-E.; Waite, J. H., Jr.; Ledvina, S. A.; Niemann, H. B.; Yelle, R. V.; Kasprzak, W. T.; Luhmann, J. G.; McNutt, R. L.; Ip, W.-H.; De La Haye, V.; Müller-Wodarg, I.; Young, D. T.; Coates, A. *J. Geophys. Res. Lett.* **2005**, *32*, L12108.

(10) Galand, M.; Lilensten, J.; Toublanc, D.; Maurice, S. *Icarus* **1999**, *140*, 92.

(11) Banaszkiewicz, M.; Lara, L. M.; Rodrigo, R.; López-Moreno, J. J.; Molina-Cuberos, G. J. *Icarus* **2000**, *147*, 386.

(12) Lilensten, J.; Simon, C.; Witasse, O.; Dutuit, O.; Thissen, R.; Alcaraz, C. *Icarus* **2005**, *174*, 285.

(13) Capone, L. A.; Dubach, J.; Whitten, R. C.; Prasad, S. S.; Santhanam, K. *Icarus* **1980**, *44*, 72.

(14) Capone, L. A.; Prasad, S. S.; Huntress, W. T.; Whitten, R. C.; Doubach, J.; Santhanam, K. *Nature* **1981**, *293*, 45.

(15) Anicich, V. G.; Milligan, D. B.; Fairley, D. A.; McEwan, M. J. *Icarus* **2000**, *146*, 118.

(16) Anicich, V. G.; Wilson, P. F.; McEwan, M. J. *J. Am. Soc. Mass Spectrom.* **2003**, *14*, 900.
(17) Anicich, V. G.; Wilson, P. F.; McEwan, M. J. *J. Am. Soc. Mass Spectrom.* **2004**, *15*, 1148.
(18) Anicich, V. G.; McEwan, M. J. *J. Am. Soc. Mass Spectrom.* **2006**, *17*, 544.
(19) Redondo, P.; Pauzat, F.; Ellinger, Y. *Planetary Space Sci.* **2006**, *54*, 181.
(20) Marco, D. S.; Marzio, R.; Antonio, S. *Chem. Phys.* **2004**, *297*, 121.
(21) Frisch, M. J.; Trucks, G. W.; Schlegel, H. B.; et al. *GAUSSIAN 98*, Revision A.6; Gaussian, Inc.: Pittsburgh, PA, 1998.
(22) Becke, A. D. *J. Chem. Phys.* **1993**, *98*, 5648.
(23) (a) Gonzalez, C.; Schlegel, H. B. *J. Chem. Phys.* **1989**, *90*, 2154. (b) Gonzalez, C.; Schlegel, H. B. *J. Chem. Phys.* **1990**, *94*, 5523.
(24) Pople, J. A.; Head-Gordon, M.; Raghavachari, K. *J. Chem. Phys.* **1987**, *87*, 5968.
(25) Mousis, O.; Gautier, D.; Coustenis, A. *Icarus* **2002**, *159*, 156.